



# Lagrange-method-based dynamic analysis of multi-stage planetary roller screw mechanism

Xin Li<sup>1</sup>, Geng Liu<sup>1</sup>, Xiaojun Fu<sup>1,2</sup>, and Shangjun Ma<sup>1</sup>

<sup>1</sup>Shaanxi Engineering Laboratory for Transmissions and Controls,  
Northwestern Polytechnical University, Xi'an, 710072, P.R. China

<sup>2</sup>School of Electrical and Electronic Engineering, University of Nottingham,  
Nottingham, NG7 2RD, UK

**Correspondence:** Geng Liu (npuliug@nwpu.edu.cn)

Received: 19 September 2020 – Revised: 30 December 2020 – Accepted: 12 February 2021 – Published: 7 May 2021

**Abstract.** A rigid-body dynamic model of multi-stage planetary roller screw mechanism (multi-stage PRSM) is proposed in this paper. The structure of multi-stage PRSM is introduced and the motion analysis is presented. The total kinetic energy of the mechanism is calculated. The rotation of the screws and carriers is chosen as generalized degrees of freedom. The generalized forces and motion equations of multi-stage PRSM are derived using the Lagrange method. The transient and steady-state behaviours of multi-stage PRSM are simulated, followed by an analysis of the influence of friction coefficients and thread pitches on the motion and forces acting on the multi-stage PRSM. Taking a two-stage PRSM as an example, the simulation results show that the friction coefficient between screw #1 and screw #2 has a slight effect on efficiency and rotational velocity ratios of carriers to screws. When the sum of the pitches of screws is a constant, the axial component of contact force between screw #1 and roller #1 decreases with the increase in the pitch of screw #1.

## 1 Introduction

Multi-stage planetary roller screw mechanism (PRSM) is a mechanical device which consists of several single-stage PRSMs for converting rotational motion into long-stroke linear motion. The mechanism has the advantage of giving an increased linear stroke for nearly the same closed length as a single-stage PRSM. As the axial motion of the nut can be transferred to the screw in the multi-stage PRSM, its output speed is much higher than the single-stage PRSM. It also has the advantages of high carrying capacity, long lifetime and high stiffness. Thus, the multi-stage PRSM is better suited to long stroke applications that require high loads and high speed, such as in the vehicle, metallurgy and chemical industries.

Despite the importance of the multi-stage PRSM, there is little fundamental research to support its engineering application. Most of the previously published papers have focused on the single-stage PRSM. These papers addressed meshing characteristics (Jones et al., 2013; Fu et al., 2017; Sandu et al., 2018), load distribution (Zhang et al., 2016;

Abevi et al., 2016), kinematic analysis (Jones and Velinsky, 2012), lubrication and wear (Auregan et al., 2015; Xie et al., 2019), manufacturing (Zhang et al., 2015), and thermal modelling (Qiao et al., 2019). According to the bond-graph formalism, Karm et al. (2009) developed a simplified dynamic model of the inverted PRSM and integrated it into a model of electromechanical actuator. Considering the elastic contacts between parts, Morozov et al. (2017) proposed a dynamic model of the PRSM to calculate the natural frequencies of the mechanism and a linear electromechanical actuator with the PRSM. Ma et al. (2017) proposed a dynamic model of PRSM based on the bond graph theory that accounts for friction forces, axial clearances, and the stiffness of the screw. Qiao et al. (2017) developed a dynamic model of the inverted PRSM in AMESim software, and the model was used to analyse the dynamic response of electromechanical brake system. Badrinarayanan et al. (2018) regarded the PRSM as a screw–nut transmission system and derived a motion equation of the PRSM. Using the Lagrange method and a viscous friction model, Jones et al. (2016) derived the mo-

tion equations of single-stage PRSM and found that the carrier rotational velocity obtained from a dynamic model was slightly slower than that from an ideal kinematic model. In order to calculate the forces acting among the screw, roller, nut and carrier, Fu et al. (2018) developed a rigid-body dynamic model of single-stage PRSM based on Newton’s second law. Fu et al. (2020) then proposed an efficient dynamic model by combing the Lagrange method and Newton’s second law to reduce computation time. Wu et al. (2020) developed a purely torsional model of the PRSM and examined the relationship between nature frequencies and the number of rollers.

Although the above studies have made significant contributions to the performance analysis of single-stage PRSM, some issues need to be addressed for better understanding of the dynamics performance of multi-stage PRSM. Firstly, the torques and forces acting on different single-stage PRSMs are different and related to each other. Secondly, the number of parts in multi-stage PRSM is greater than in single-stage PRSM. An efficient dynamic model should be developed to avoid solving a large number of nonlinear equations. Lastly, the influence of connections between different single-stage PRSMs on the dynamics of multi-stage PRSM needs to be studied.

Based on the issues mentioned above, a rigid-body dynamic model of multi-stage PRSM is proposed in this study by using the Lagrange method. The total kinetic energy of the mechanism is given after the motion analysis. The generalized forces corresponding to the rotation of the screw and carriers are derived by taking the friction forces at the screw–roller and screw–screw interfaces into consideration. Then, the motion equations of multi-stage PRSM are developed. Lastly, an example is provided to show the transient and steady-state behaviours of multi-stage PRSM. The influence of friction coefficients and the pitches of threads on the motion and forces acting on the multi-stage PRSM is also analysed and discussed.

## 2 Modelling

### 2.1 Kinetic energy

As shown in Fig. 1, the multi-stage PRSM mainly consists of screws, nuts, rollers, carriers and ring gears. The symbol  $k$  denotes the  $k$ th stage ( $k = 1, 2, \dots, n_T$ ,  $n_T$  is the number of stages in the multi-stage PRSM). In Fig. 1,  $n_T = 2$ . The axial motion of nut  $\#(k - 1)$  is transferred to screw  $\#k$  by two thrust bearings. The global coordinate system is fixed in space with its  $Z$  axis coincident with the axis of screw  $\#1$ . As screw  $\#(k - 1)$  and screw  $\#k$  are connected by the splined shaft shown in Fig. 1, the rotational velocities of screw  $\#k$  ( $k > 1$ )  $\dot{\theta}_{S_k}$  are the same:

$$\dot{\theta}_{S_k} = \dot{\theta}_S \quad (k = 1, 2, \dots, n_T), \tag{1}$$

where  $\dot{\theta}_S$  is the given rotational velocity of the screw.

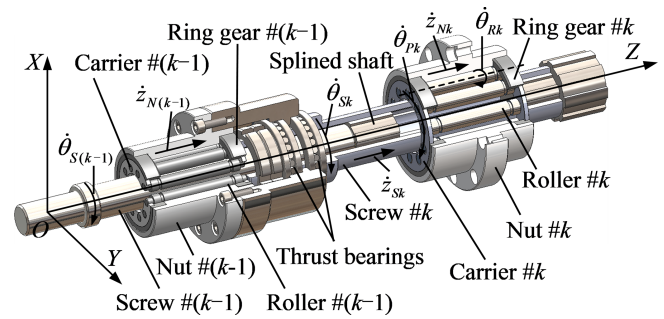


**Figure 1.** Structure and motion analysis of the multi-stage planetary roller screw mechanism (multi-stage PRSM).

In this paper, screws, rollers and nuts are assumed to be right-handed and the axial velocity of nut  $\#k$   $\dot{z}_{Nk}$  is given as

$$\dot{z}_{Nk} = -\frac{\dot{\theta}_S}{2\pi} \sum_{i=1}^k L_{Si}, \tag{2}$$

where  $L_{Si}$  is the lead of screw  $\#i$  and  $i = 1, 2, \dots, k$ . Then, the axial velocity of screw  $\#k$  ( $k > 1$ )  $\dot{z}_{Sk}$  can be given as

$$\dot{z}_{Sk} = \dot{z}_{N(k-1)} \quad (k > 1), \tag{3}$$

where  $\dot{z}_{N(k-1)}$  is the axial velocity of nut  $\#(k - 1)$ .

When screws are rotating, rollers are rolling inside nuts. If the rotational velocities of rollers about the screw axis are the same and are equal to those of carriers, the velocity at the centre of roller  $\#k$   $v_{Rk}$  is calculated as

$$v_{Rk} = \sqrt{\dot{\theta}_{P_k}^2 (r_{S_k} + r_{R_k})^2 + \dot{z}_{N_k}^2}, \tag{4}$$

where  $\dot{\theta}_{P_k}$  is the rotational velocity of carrier  $\#k$ , and  $r_{S_k}$  and  $r_{N_k}$  are the nominal radii of screw  $\#k$  and roller  $\#k$ .

Referring to the kinematic analysis given by Jones and Velinsky (2012), the rotational velocity of roller  $\#k$   $\dot{\theta}_{Rk}$  about its axis can be expressed as

$$\dot{\theta}_{Rk} = -(n_{S_k} - 1)\dot{\theta}_{P_k}, \tag{5}$$

where  $n_{S_k}$  is the number of starts on the thread of screw  $\#k$ .

Using Eqs. (1)–(3), the kinetic energy of screws  $T_S$  in the multi-stage PRSM can be derived as

$$T_S = \frac{1}{2} \sum_{k=1}^{n_T} (J_{S_k} \dot{\theta}_{S_k}^2) + \frac{1}{2} \sum_{k=2}^{n_T} (m_{S_k} \dot{z}_{N(k-1)}^2), \tag{6}$$

where  $J_{S_k}$  and  $m_{S_k}$  are the moment of inertia and the mass of screw  $\#k$ . As the rotation of all nuts shown in Fig. 1 is constrained, the kinetic energy of nuts  $T_N$  is

$$T_N = \frac{1}{2} \sum_{k=1}^{n_T} (m_{N_k} \dot{z}_{N_k}^2), \tag{7}$$

where  $m_{N_k}$  is the mass of nut  $\#k$ .

According to the motion analysis shown in Fig. 1, the kinetic energy of carriers  $T_P$  is written as

$$T_P = \frac{1}{2} \sum_{k=1}^{n_T} (2J_{Pk} \dot{\theta}_{Pk}^2) + \frac{1}{2} \sum_{k=1}^{n_T} (2m_{Pk} \dot{z}_{Nk}^2), \quad (8)$$

where  $J_{Pk}$  and  $m_{Pk}$  are the moment of inertia and the mass of carrier  $\#k$ . The kinetic energy of rollers  $T_R$  is derived as

$$T_R = \frac{1}{2} \sum_{k=1}^{n_T} (N_{Rk} J_{Rk} \dot{\theta}_{Rk}^2) + \frac{1}{2} \sum_{k=1}^{n_T} (N_{Rk} m_{Rk} \dot{v}_{Rk}^2), \quad (9)$$

where  $N_{Rk}$  is the total number of roller  $\#k$ , and  $J_{Rk}$  and  $m_{Rk}$  are the moment of inertia and the mass of roller  $\#k$ . Then, the total kinetic energy of the multi-stage PRSM  $T_{total}$  is

$$T_{total} = T_S + T_N + T_P + T_R. \quad (10)$$

Substituting Eqs. (6)–(9) into Eq. (10), the total kinetic energy  $T_{total}$  can be expressed as a function of the rotational velocities of the screw and carriers:

$$T_{total} = \frac{1}{2} \dot{\theta}_S^2 \sum_{k=1}^{n_T} \left[ J_{Sk} + \left( \frac{1}{2\pi} \sum_{i=1}^k L_{Si} \right)^2 (m_{Nk} + 2m_{Pk} + N_{Rk} m_{Rk}) \right] + \frac{\dot{\theta}_S^2}{8\pi^2} \sum_{k=2}^{n_T} m_{Sk} \left( \sum_{i=1}^{k-1} L_{Si} \right)^2 + \frac{1}{2} \sum_{k=1}^{n_T} \dot{\theta}_{Pk}^2 \left[ 2J_{Pk} + N_{Rk} J_{Rk} (n_{Sk} - 1)^2 + N_{Rk} m_{Rk} (r_{Sk} + r_{Rk})^2 \right]. \quad (11)$$

### 2.2 Generalized forces and motion equations

As shown in Fig. 2,  $M_{Sk}$  and  $f_{Sk}$  are the driven torque and the friction force acting on the internal spline teeth of screw  $\#k$ .  $F_{Nk}$  is the external force acting on nut  $\#k$ , and  $f_{Srk}$  is the friction force between screw  $\#k$  and roller  $\#k$ .  $O_{Pk-x_{Pk}y_{Pk}z_{Pk}}$  is a local coordinate system fixed at the centre of carrier  $\#k$ .  $\phi_{Pk}$  is the angle between the  $X$  axis and  $x_{Pk}$  axis. There is no slip at the nut–roller interface if screws, rollers and nuts are regarded as rigid bodies, and manufacturing and assembly errors are not included. Besides, the friction coefficients in thrust bearings are usually very small. Hence, the friction force at the nut–roller interface and that in thrust bearings are ignored in this paper. When the driven torque  $M_{Sk}$  is given, the friction force  $f_{Sk}$  can be expressed as

$$f_{Sk} = \mu_{SS} \frac{|M_{Sk}|}{r_{SSk}} \text{sign}(\dot{\theta}_S) \quad (k > 1), \quad (12)$$

where  $\mu_{SS}$  is the friction coefficient between external and internal spline teeth, and  $r_{SSk}$  is the nominal radius of internal

spline teeth on screw  $\#k$ .  $\text{sign}()$  is a symbolic function, and  $\text{sign}(\dot{\theta}_S)$  is defined as

$$\text{sign}(\dot{\theta}_S) = \begin{cases} 1 & \dot{\theta}_S > 0 \\ 0 & \dot{\theta}_S = 0 \\ -1 & \dot{\theta}_S < 0 \end{cases}. \quad (13)$$

As mentioned by Fu et al. (2018), the slip velocity between screw  $\#k$  and roller  $\#k$  can be represented in the local coordinate system  $O_{Pk-x_{Pk}y_{Pk}z_{Pk}}$  as

$$\mathbf{v}_{Rsk}^{Pk} = \begin{bmatrix} -r_{Srk}(\dot{\theta}_S - \dot{\theta}_{Pk}) \sin \varphi_{Srk} - n_{Sk} \dot{\theta}_{Pk} r_{Rsk} \sin \varphi_{Rsk} \\ r_{Srk}(\dot{\theta}_S - \dot{\theta}_{Pk}) \cos \varphi_{Srk} - n_{Sk} \dot{\theta}_{Pk} r_{Rsk} \cos \varphi_{Rsk} \\ \dot{\theta}_S L_{Sk} / (2\pi) \end{bmatrix}, \quad (14)$$

where  $r_{Srk}$ ,  $r_{Rsk}$ ,  $\varphi_{Srk}$  and  $\varphi_{Rsk}$  are the contact radii and angles at the screw–roller interface, which can be obtained from the model developed by Fu et al. (2017). According to Coulomb’s law, the friction force  $f_{Srk}$  is

$$\mathbf{f}_{Srk} = \begin{bmatrix} f_{Srxk} \\ f_{Sryk} \\ f_{Srz k} \end{bmatrix} = \mathbf{H}_{Pk} \cdot \mu_{SR} F_{Srk} \frac{(-\mathbf{v}_{Rsk}^{Pk})}{\|\mathbf{v}_{Rsk}^{Pk}\|}, \quad (15)$$

where  $f_{Srxk}$ ,  $f_{Sryk}$  and  $f_{Srz k}$  are the  $X$ ,  $Y$  and  $Z$  components of the friction force  $\mathbf{f}_{Srk}$ ,  $\mu_{SR}$  is the friction coefficient at the screw–roller interface,  $F_{Srk}$  is the contact force between screw  $\#k$  and roller  $\#k$ , and  $\mathbf{H}_{Pk}$  is the rotational matrix relating to the global coordinate system  $O-XYZ$  and local coordinate system  $O_{Pk-x_{Pk}y_{Pk}z_{Pk}}$ :

$$\mathbf{H}_{Pk} = \begin{bmatrix} \cos \phi_{Pk} & \sin \phi_{Pk} & 0 \\ -\sin \phi_{Pk} & \cos \phi_{Pk} & 0 \\ 0 & 0 & 1 \end{bmatrix}. \quad (16)$$

Based on the Lagrange method, the generalized force corresponding to the rotational velocity of the screw  $\dot{\theta}_S$  can be given as

$$G_S = F_{N(n_T)} \cdot \frac{\partial \dot{z}_{N(n_T)}}{\partial \dot{\theta}_S} + M_{S1} \cdot \frac{\partial \dot{\theta}_{S1}}{\partial \dot{\theta}_S} + \sum_{k=1}^{n_T} \left[ N_{Rk} \mathbf{f}_{Srk}^T \cdot \frac{\partial (\mathbf{H}_{Pk} \mathbf{v}_{Rsk}^{Pk})}{\partial \dot{\theta}_S} \right] + \sum_{k=2}^{n_T} \left( f_{Sk} \cdot \frac{\partial \dot{z}_{Sk}}{\partial \dot{\theta}_S} \right), \quad (17)$$

where  $F_{N(n_T)}$  is the external force acting on the last nut,  $M_{S1}$  is the driven torque acting on screw  $\#1$  and  $\mathbf{v}_{Rsk}^{Pk}$  is the velocity of the contact point on screw  $\#k$  represented in the local coordinate system  $O_{Pk-x_{Pk}y_{Pk}z_{Pk}}$  as

$$\mathbf{v}_{Rsk}^{Pk} = [-\dot{\theta}_S r_{Srk} \sin \varphi_{Srk} \quad \dot{\theta}_S r_{Srk} \cos \varphi_{Srk} \quad 0]^T. \quad (18)$$

The generalized force corresponding to the rotational velocity of carrier  $\#k$  is

$$G_{Pk} = N_{Rk} (-\mathbf{f}_{Srk})^T \cdot \frac{\partial (\mathbf{H}_{Pk} \mathbf{v}_{Rk}^{Pk})}{\partial \dot{\theta}_{Pk}}, \quad (19)$$

where  $v_{Rk}^{Pk}$  is the velocity of the contact point on roller # $k$  represented in the local coordinate system  $O_{Pk}-x_{Pk}y_{Pk}z_{Pk}$  as

$$v_{Rk}^{Pk} = \begin{bmatrix} \dot{\theta}_{Pk}(-r_{Srk} \sin \varphi_{Srk} + n_s r_{Rsk} \sin \varphi_{Rsk}) \\ \dot{\theta}_{Pk}(r_{Srk} \cos \varphi_{Srk} + n_s r_{Rsk} \cos \varphi_{Rsk}) \\ -(\dot{\theta}_S L_{Sk}) / (2\pi) \end{bmatrix}, \quad (20)$$

where  $L_{Sk}$  is the lead of screw # $k$ .

Using the total kinetic energy shown in Eq. (11) and the generalized forces given in Eqs. (17) and (19), the motion equation of the multi-stage PRSM is given as

$$\begin{cases} \frac{d}{dt} \left( \frac{\partial T_{total}}{\partial \dot{\theta}_S} \right) - \frac{\partial T_{total}}{\partial \theta_S} = G_S \\ \frac{d}{dt} \left( \frac{\partial T_{total}}{\partial \dot{\theta}_{Pk}} \right) - \frac{\partial T_{total}}{\partial \theta_{Pk}} = G_{Pk} \end{cases}, \quad (21)$$

and Eq. (21) can be rewritten as

$$\begin{cases} G_S = \ddot{\theta}_S^2 \sum_{k=1}^{n_T} \left[ J_{Sk} + \left( \frac{1}{2\pi} \sum_{i=1}^k L_{Si} \right)^2 (m_{Nk} + 2m_{Pk} + N_{Rk}m_{Rk}) \right] \\ \quad + \frac{\ddot{\theta}_S^2}{4\pi^2} \sum_{k=2}^{n_T} m_{Sk} \left( \sum_{i=1}^k L_{Si} \right)^2 \\ G_{Pk} = \ddot{\theta}_{Pk}^2 \left[ 2J_{Pk} + N_{Rk}J_{Rk}(n_S - 1)^2 \right. \\ \quad \left. + N_{Rk}m_{Rk}(r_{Sk} + r_{Rk})^2 \right] \end{cases}. \quad (22)$$

The motion equation shown in Eq. (22) includes  $(n_T+1)$  nonlinear equations. As the contact force,  $F_{Srk}$ , between screw # $k$  and roller # $k$  and the driven torque,  $M_{Sk}$ , acting on the internal spline teeth of screw # $k$  are not given, more equations should be added in order to solve Eq. (22).

According to the equilibrium of the torques and forces acting on screw # $k$ , the rotational and translational motion equations of screw # $k$  are

$$J_{Sk} \ddot{\theta}_S = r_{Srk} (f_{Sryk} \cos \varphi_{Srk} - f_{Srxk} \sin \varphi_{Srk}) + M_{Sk} - M_{S(k+1)}, \quad (23)$$

$$m_{Sk} \ddot{z}_{Sk} = -F_{N(k-1)} + f_{Sk} - f_{S(k+1)} + f_{Srz} + F_{Srz}, \quad (24)$$

where  $F_{Srz}$  is the axial component of the contact force between screw # $k$  and roller # $k$  and can be given as

$$F_{Srz} = \frac{F_{Srk}}{\sqrt{1 + \tan^2 \beta_{Sk} + [L_{Sk} / (2\pi r_{Srk})]^2}}, \quad (25)$$

where  $\beta_{Sk}$  is the flank angle of screw # $k$ .

Similarly, the motion equation corresponding to the axial translation of roller # $k$  and nut # $k$  is given as

$$\left( m_{Rk} + \frac{m_{Nk}}{N_{Rk}} \right) \ddot{z}_{Nk} = -f_{Srz} - F_{Srz} + \frac{F_{Nk}}{N_{Rk}}, \quad (26)$$

where  $F_{Nk}$  is the external force acting on nut # $k$  and  $N_{Rk}$  is the total number of roller # $k$ . There are  $(4n_T - 1)$  unknowns in Eqs. (22)–(26) which provide  $(4n_T - 1)$  nonlinear equations. The motion and the forces acting on roller # $k$ , screw # $k$  and nut # $k$  in the multi-stage PRSM can be obtained by solving Eqs. (22)–(26).

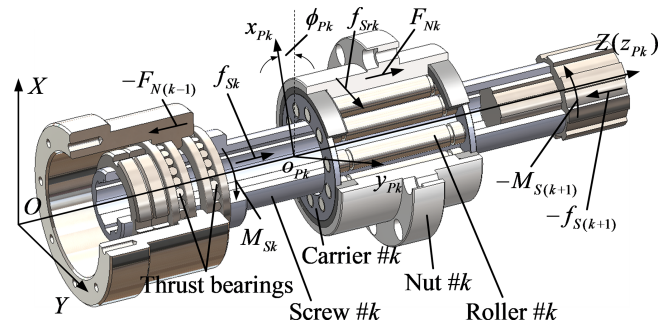


Figure 2. Force analysis of the  $k$ th stage in the multi-stage PRSM.

### 3 Results and discussion

#### 3.1 Transient and steady-state behaviours

A two-stage PRSM ( $n_T = 2$ ) is used as an example in this section. The structural and mass parameters of screw #1, nut #1, roller #1 and carrier #1 are given as follows. The nominal radii of screw #1, roller #1 and nut #1 are  $r_{S1} = 9.75$ ,  $r_{R1} = 3.25$  and  $r_{N1} = 16.25$  mm, respectively. The lead, start number and flank angle of screw #1 are  $L_{S1} = 10$  mm,  $n_{S1} = 5$  and  $\beta_{S1} = 45^\circ$ , respectively. The total number of roller #1 is  $N_{R1} = 7$ . The mass of roller #1 and nut #1 are  $m_{R1} = 0.017$  and  $m_{N1} = 2.5$  kg. The inertia moments of screw #1, roller #1 and carrier #1 are  $J_{S1} = 55$ ,  $J_{R1} = 0.08$  and  $J_{P1} = 3$  kg mm<sup>2</sup>, respectively. The structural and mass parameters of screw #2, nut #2, roller #2 and carrier #2 are  $r_{S2} = 16.5$ ,  $r_{N2} = 27.5$ ,  $r_{R2} = 5.5$ ,  $n_{S2} = 5$ ,  $L_{S2} = 10$ ,  $\beta_{S2} = 45^\circ$ ,  $N_{R2} = 7$ ,  $m_{S2} = 0.77$ ,  $m_{N2} = 18$ ,  $m_{R2} = 0.04$  kg,  $J_{S2} = 170$ ,  $J_{R2} = 0.48$  and  $J_{P2} = 12$  kg mm<sup>2</sup>. The nominal radius of internal spline teeth on screw #2 is  $r_{SS2} = 13$  mm.

When the external force acting on nut #2 is  $F_{N2} = 5000$  N, and the rotational velocity of the screw is  $100$  rad s<sup>-1</sup>. The transient and steady-state behaviours of the two-stage PRSM are shown in Fig. 3a–d. In Fig. 3a,

$$\zeta_{PSk} = \frac{\dot{\theta}_{Pk}}{\dot{\theta}_S} \quad (k = 1 \text{ or } 2), \quad (27)$$

where  $\zeta_{PSk}$  is the rotational velocity ratio of carrier # $k$  to the screw.

Because the axial movement of screw #2 is driven by nut #1 in the two-stage PRSM, the contact force at the screw#1–roller #1 interface is larger than at the screw #2–roller #2 interface. Thus, the slope of  $\zeta_{PS1}$  is steeper than that of  $\zeta_{PS2}$  before the steady state is reached, as shown in Fig. 3a. It takes carrier #1 about 0.14 ms to reach at the steady state. After  $t = 0.46$  ms, carrier #2 reaches at the steady state and the value of  $\zeta_{PS2}$  is larger than that of  $\zeta_{PS1}$ . Because the helix angle of screw #2 is smaller than that of screw #1, the contact point at the screw #2–roller #2 interface is closer to the point of tangency between their pitch circles. This will reduce the slip between screw #2 and roller #2. When the rotational velocity of carrier # $k$  increases, the tangential component of the

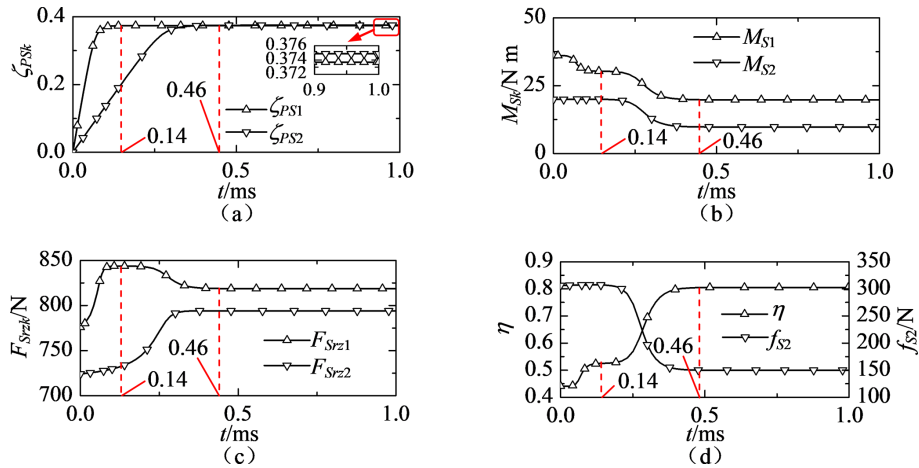


**Figure 3.** Transient and steady-state behaviours of the two-stage PRSM: (a) rotational velocity ratios, (b) driven torque acting on screw #*k*, (c) axial component of the contact force at the screw #*k*–roller #*k* interface, (d) efficiency and friction force between screw #2 and screw #1.

slip velocity  $v_{R_{S_k}}^{P_k}$  and the friction torque acting on screw #*k* decrease. Therefore, the values of driven torques,  $M_{S1}$  and  $M_{S2}$ , at the beginning of the simulation are larger than those at the steady state, as shown in Fig. 3b. As the rotational movement of screw #2 is driven by screw #1, the value of  $M_{S1}$  is much larger than that of  $M_{S2}$  all the time. It should be noticed that the nominal radius of screw #1 is smaller than that of screw #2. After  $t = 0.14$  ms, the value of  $M_{S2}$  remains stable for a short time and then reduces to the steady-state value. The difference between the values of  $M_{S1}$  and  $M_{S2}$  is the largest at  $t = 0$  ms.

The axial component of the friction force between screw #*k* and roller #*k* increases when the rotational velocity of carrier #*k* increases. This will lead to the increase of the contact force between screw #*k* and roller #*k*, as shown in Fig. 3c. Because the value of  $F_{S_{rz1}}$  is also influenced by the friction force at the screw #1–screw#2 interface, it decreases when the driven torque of screw #2 decreases. The contact force between screw #1 and roller #1 is always larger than between screw #2 and roller #2. In Fig. 3d, the efficiency  $\eta$  is expressed as

$$\eta = \frac{F_{N2}(L_{S1} + L_{S2})}{2\pi M_{S1}}, \tag{28}$$

where  $F_{N2}$  is the external force of acting on nut #2 and  $M_{S1}$  is the driven torque acting on screw #1.

As shown in Fig. 3d, the efficiency of the two-stage PRSM is less than 0.45 at the beginning of the simulation and it increases nearly to 0.80 at the steady state. This is because that the driven torque of screw #1 decreased during the simulation. The friction force between screw #1 and screw #2 is also as shown in Fig. 3d. According to Eq. (12), the value of friction force varies with changes in the driven torque of screw #2. Thus, the change of  $f_{S2}$  in Fig. 3d is similar to that of  $M_{S2}$  in Fig. 3b.

### 3.2 Influence of friction coefficients

When the friction coefficient between the screw and roller is 0.1 or 0.2, and that between screw #1 and screw #2 is 0.2 or 0.3, the transient and steady-state behaviours of the two-stage PRSM are as shown in Fig. 4a–d.

Because the rolling of rollers is driven by friction forces at the screw–roller interface, the slope of  $\zeta_{P_{S1}}$  or  $\zeta_{P_{S2}}$  increases with the increase in  $\mu_{SR}$ , as shown in Fig. 4a. The friction coefficient between screw #1 and screw #2 has a slight effect on the values of  $\zeta_{P_{S1}}$  and  $\zeta_{P_{S2}}$ . According to Eqs. (15), (19) and (22), the friction forces at the screw–roller interface and the external forces acting on nuts have no influence on the values of  $\zeta_{P_{S1}}$  and  $\zeta_{P_{S2}}$  when the rotational accelerations of carriers #1 and #2 are zero. As shown in Fig. 4a, the values of  $\zeta_{P_{S1}}$  and  $\zeta_{P_{S2}}$  remain steady at the steady state under different friction coefficients. As shown in Fig. 4b, the contact forces between the screw and rollers increase when the friction coefficient between threads is increased. The axial components of friction forces at the screw–roller interface have greater influence on the contact forces at the interface than the tangential components. The difference between the contact force at  $t = 0$  and  $t = 0.75$  ms also increases with the increase in the friction coefficient between threads, as shown in Fig. 4b. Because the forces acting on the splined shaft can not affect the forces acting on roller #2, the contact force between screw #2 and roller #2 is independent from the friction coefficient between screw #1 and screw #2.

As Fig. 4c shows, the efficiency decreases with the increase in the friction coefficient at the screw–roller interface. Meanwhile, the friction coefficient between screw #1 and screw #2 has a slight effect on the efficiency. This is because the friction force between screw #1 and screw #2, as shown in Fig. 4d, is much smaller than the external force acting on nut #2. Besides, the increase of the friction coefficient at screw #1 and screw #2 can only lead to a small increase

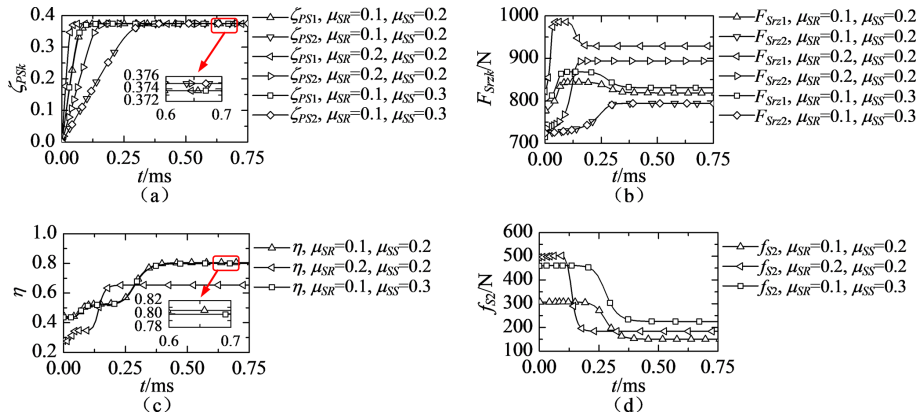


**Figure 4.** Influence of friction coefficients on (a) rotational velocity ratios, (b) axial component of the contact force at the screw #*k*–roller #*k* interface, (c) efficiency and (d) friction force between screw #2 and screw #1.

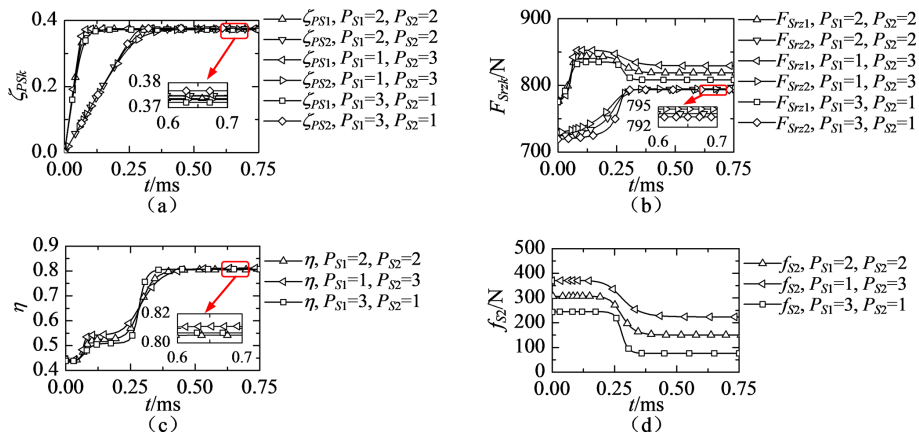


**Figure 5.** Influence of thread pitches on (a) rotational velocity ratios, (b) axial component of the contact force at the screw #*k*–roller #*k* interface, (c) efficiency and (d) friction force between screw #2 and screw #1.

in the contact force at the screw #1 and the roller #1 interface, as shown in Fig. 4b. As Fig. 4d shows, the friction force between screw #1 and screw #2 increases with the increase in the friction coefficients. This is because the driven torque acting on screw #2 is influenced by the friction force between screw #2 and roller #2. As Fig. 4d shows, the friction coefficient between the screw and rollers has greater influence on the value of  $f_{S2}$  at the beginning of simulation, and that between screws #1 and #2 has greater influence on the value of  $f_{S2}$  at the steady state.

### 3.3 Influence of thread pitches

When the sum of pitches of screw #1 and screw #2 is equal to 4 mm and those are chosen from 1 to 3 mm, the transient and steady-state behaviours of the two-stage PRSM are as shown in Fig. 5a–d.

When the thread pitches decrease, the tangential components of friction forces at the screw–roller interface increase and the contact point on the screw is close to the point of

tangency between pitch circles. As shown in Fig. 5a, when the pitch of screw #1 is decreased, it takes  $\zeta_{PS1}$  less time to reach at the steady state, followed by an increase in steady-state value of  $\zeta_{PS1}$ . The change of the curve of  $\zeta_{PS2}$  in Fig. 5a is similar to that of  $\zeta_{PS1}$ . As shown in Fig. 5b, the contact force at the screw #2–roller #2 interface slightly increases when the pitch of screw #2 is increased. This is because the axial component of the friction force at the screw #2–roller #2 interface increases with the increase in the pitch of screw #2 and the pitch of screw #1 has no effect on the friction force. The increase of the pitch of screw #2 leads to the increase in the driven torque acting on screw #2. It enlarges the friction force between screw #1 and screw #2, as shown in Fig. 5d. By comparing Fig. 5b and d, it can be found that the influence of the pitch of screw #2 on the friction force at the screw #1 and the screw #2 interface is much greater than at the screw #2–roller #2 interface. Therefore, the value of  $F_{Sr21}$  decreases when the pitch of screw #1 is increased.

As shown in Fig. 5c, the pitches of screws have slight influence on the steady-state efficiency of the two-stage PRSM

when the sum of pitches is a constant. It should be noticed that if the length of a roller is a constant, the number of thread teeth on the roller will increase with the decrease in the thread pitch. Therefore, the pitch of screw #1 can be smaller than that of screw #2 in order to reduce the contact forces acting on thread teeth at the screw #1–roller #1 interface. As shown in Fig. 5c, the value of  $f_{S2}$  increases with the increase in the pitch of screw #2.

## 4 Conclusions

A rigid-body dynamic model of multi-stage planetary roller screw mechanism (PRSM) has been proposed in this paper. A structure and motion analysis of multi-stage PRSM were presented, and the total kinetic energy of the mechanism was calculated. The generalized forces corresponding to the rotational movements of the screw and carriers were derived by using the Lagrange method. The motion equations of multi-stage PRSM were developed. Based on the examples provided in this paper, several conclusions are listed below.

Although the nominal radius of screw #1 is smaller than that of screw #2, the driven torque and contact force acting on screw #1 are larger than those acting on screw #2. It will take carrier #2 more time than carrier #1 to reach at the steady state. When the pitches of screw #1 and screw #2 are the same, the rotational velocity of carrier #2 is larger than that of carrier #1 at the steady state.

The efficiency of the two-stage PRSM decreases with the increase in the friction coefficient at the screw–roller interface. The friction coefficient between screw #1 and screw #2 has a slight effect on the efficiency. These friction coefficients have no effect on the rotational velocities of carriers. The friction coefficient between the screw and rollers has greater influence on the friction force between screw #1 and screw #2 at the beginning of simulation.

When the sum of the pitches of screw #1 and screw #2 is a constant, the pitches have little influence on the efficiency of the two-stage PRSM. The influence of the pitch of screw #2 on the friction force at the screw #1–screw #2 interface is much greater than at the screw #2–roller #2 interface. The axial component of contact force between screw #1 and roller #1 decreases with the increase in the pitch of screw #1.

**Data availability.** All data, models, and codes generated or used during the study are available from the corresponding author upon request.

**Author contributions.** XL proposed the theory of the modelling method, analysed numerical results and wrote the paper; GL provided guidance on theoretical methods and edited the manuscript; XF prepared the figures; SM edited the manuscript.

**Competing interests.** The authors declare that they have no conflict of interest.

**Special issue statement.** This article is part of the special issue “Robotics and advanced manufacturing”. It is not associated with a conference.

**Acknowledgements.** We would like to thank David Bowen for providing the language help in this paper.

**Financial support.** This research has been supported by the National Natural Science Foundation of China (grant nos. 51905428, 51875458, 51535009), the Natural Science Basic Research Plan in Shaanxi Province of China (grant no. 2020JQ-178), and the China Scholarship Council (grant nos. 202006290149 and 201906295012).

**Review statement.** This paper was edited by Guimin Chen and reviewed by four anonymous referees.

## References

- Abevi, F., Daidie, A., Chaussumier, M., and Sartor, M.: Static load distribution and axial stiffness in a planetary roller screw mechanism, *J. Mech. Des.-T. ASME*, 138, 1–11, <https://doi.org/10.1115/1.4031859>, 2016.
- Auregan, G., Fridrici, V., Kapsa, P., and Rodrigues, F.: Experimental simulation of rolling-sliding contact for application to planetary roller screw mechanism, *Wear*, 332–333, 1176–1184, <https://doi.org/10.1016/j.wear.2015.01.047>, 2015.
- Badrinarayanan, S., Kumar, V. R., and Bhinder, K. S.: Electro mechanical linear actuator using roller screws, *IOP Conf. Ser.-Mat. Sci.*, 402, 1–10, <https://doi.org/10.1088/1757-899X/402/1/012101>, 2018.
- Fu, X. J., Liu, G., Ma, S. J., Tong, R. T., and Lim, T. C.: A comprehensive contact analysis of planetary roller screw mechanism, *J. Mech. Des.-T. ASME*, 139, 1–11, <https://doi.org/10.1115/1.4034580>, 2017.
- Fu, X. J., Liu, G., Tong, R. T., Ma, S. J., and Lim, T. C.: A nonlinear six degree of freedom dynamic model of planetary roller screw mechanism, *Mech. Mach. Theory*, 119, 22–36, <https://doi.org/10.1016/j.mechmachtheory.2017.08.014>, 2018.
- Fu, X. J., Liu, G., Ma, S. J., Tong, R. T., and Li, X.: An efficient method for the dynamic analysis of planetary roller screw mechanism, *Mech. Mach. Theory*, 150, 1–15, <https://doi.org/10.1016/j.mechmachtheory.2020.103851>, 2020.
- Jones, M. H. and Velinsky, S. A.: Kinematics of roller migration in the planetary roller screw mechanism, *J. Mech. Des.*, 134, 1–6, <https://doi.org/10.1115/1.4006529>, 2012.
- Jones, M. H. and Velinsky, S. A.: Contact kinematics in the roller screw mechanism, *J. Mech. Des.*, 135, 1–10, <https://doi.org/10.1115/1.4023964>, 2013.

- Jones, M. H., Velinsky, S. A., and Lasky, T. A.: Dynamics of the planetary roller screw mechanism, *J. Mech. Robot.*, 8, 1–6, <https://doi.org/10.1115/1.4030082>, 2016.
- Karm, W. and Mare, J. C.: Modelling and simulation of mechanical transmission in roller-screw, *Aircr. Eng. Aerosp. Tec.*, 81, 288–298, <https://doi.org/10.1108/00022660910967273>, 2009.
- Ma, S. J., Zhang, T., Liu, G., and He, J. P.: Bond graph-based dynamic model of planetary roller screw mechanism with consideration of axial clearance and friction, *P. I. Mech. Eng. C-J. Mec.*, 232, 2899–2911, <https://doi.org/10.1177/0954406217727631>, 2017.
- Morozov, V., Fadeev, P., Shtych, D., Belyaev, L., and Zhdanov, A.: Vibration decrease of electromechanical actuators based on roller screw mechanisms, *Matec. Web Conf.*, 129, 1–5, <https://doi.org/10.1051/mateconf/201712906026>, 2017.
- Qiao, G., Liu, G., Shi, Z. H., Wang, Y. W., Ma, S. J., and Teik, L.: Effect of friction torque on electromechanical brake system dynamics, *SAE International Journal of Vehicle Dynamics, Stability, and NVH*, 1, 471–479, <https://doi.org/10.4271/2017-01-1902>, 2017.
- Qiao, G., Liu, G., Ma, S. J., Wang, W. Y., Li, P., and Lim, T. C.: Thermal characteristics analysis and experimental study of the planetary roller screw mechanism, *Appl. Therm. Eng.*, 149, 1345–1358, <https://doi.org/10.1016/j.applthermaleng.2018.12.137>, 2019.
- Sandu, S., Biboulet, N., Nelias, D., and Abevi, F.: An efficient method for analyzing the roller screw thread geometry, *Mech. Mach. Theory*, 126, 243–264, <https://doi.org/10.1016/j.mechmachtheory.2018.04.004>, 2018.
- Wu, L. P., Ma, S. J., Wang, Q., and Liu, G.: Dynamic Model of Planetary Roller Screw Mechanism with Considering Torsional Degree of Freedom, *Matec. Web Conf.*, 306, 1–5, <https://doi.org/10.1051/mateconf/202030601003>, 2020.
- Xie, Z. J., Xue, Q. X., Wu, J. Q., Gu, L., Wang, Q. L., and Song, B. Y.: Mixed-lubrication analysis of planetary roller screw, *Tribol. Int.*, 140, 1–9, <https://doi.org/10.1016/j.triboint.2019.105883>, 2019.
- Zhang, D. W., Zhao, S. D., Wu, S. B., Zhang, Q., Fan, S. Q., and Li, J. X.: Phase characteristic between dies before rolling for thread and spline synchronous rolling process, *Int. J. Adv. Manuf. Tech.*, 81, 513–528, <https://doi.org/10.1007/s00170-015-7146-7>, 2015.
- Zhang, W. J., Liu, G., Tong, R. T., and Ma, S. J.: Load distribution of planetary roller screw mechanism and its improvement approach, *P. I. Mech. Eng. C-J. Mec.*, 230, 3304–3318, <https://doi.org/10.1177/0954406215610361>, 2016.